Three-dimensional DC resistivity finite element and finite difference forward modeling in comparison

Yuguo Li and Klaus Spitzer
Institut für Geophysik, TU Bergakademie Freiberg

1 INTRODUCTION

A limited number of numerical solutions of the three-dimensional (3D) direct current (DC) resistivity problem have been discussed in the geophysical literature. These solutions have been obtained using integral equation, finite difference or finite element techniques. The integral equation method is most efficient for modeling one or a few inhomogeneous bodies in a homogeneous earth. Finite difference (FD) and finite element (FE) methods are better suited to model any arbitrarily complex 3D earth. Dey & Morrison (1979) developed a 3D finite-difference algorithm to evaluate the potential for a point current source. The equation of continuity is integrated over elemental volumes to obtain a system of self-adjoint difference equations. A mixed boundary condition was introduced, based on the asymptotic behavior of the potential field in a homogeneous medium. Spitzer (1995) reported a FD algorithm using conjugate gradient methods. A compact storage scheme was employed, which reduced the number of memory-resident coefficients and shortened the run time by avoiding unnecessary computational operations. Lowry et al. (1989) proposed a 3D integrated finite difference scheme using a singularity removal technique. This method actually models the anomalous potential which is due to conductivity contrasts. The anomalous potential is smoother than the total potential, therefore, the solution is generally more exact. Two modifications of the finite difference method were recently made by Zhao & Yedlin (1996). The first is a more accurate formula for the source singularity removal. The second is the analytic computation of the source terms that arise from the decomposition of the potential into the primary and secondary potential. Spitzer et al. (1999) presented a 3D DC and induced polarization (IP) finite difference code, which offers grid-independent electrode positioning and detaches both transmitters and receivers from grid nodes. The discussion of the finite element method is a bit more sparse, perhaps because finite elements are more complex to implement than finite differences. The application of the finite element method to the 2D resistivity problem was discussed by Coggon (1971). A finite element solution to the 3D resistivity problem was reported by Pridmore et al. (1981). Sasaki (1994) developed a 3D resistivity inversion algorithm using the finite element method. Recently, Zhou & Greenhalgh (2001) published a finite element solution to the 3D DC problem. The mixed boundary condition and a compact storage scheme were incorporated. However, they solved the governing equation of the total potential.
In this paper, we revisited 3D FE resistivity modeling, but with the use of the singularity removal. Furthermore, a modified method of singularity removal is presented. First the theoretical basis of our FE solution for the secondary potential is developed. After that, the FE and FD schemes are compared in terms of accuracy and memory requirements. Finally, the effect of singularity removal is illustrated by three examples: a dike model, a cube buried in a two-layered earth and a cube buried near a vertical contact.

2 THE BOUNDARY VALUE PROBLEM

We assume a 3D conductivity model $\sigma(x,y,z)$ in a Cartesian system of coordinates (x,y,z) with z positive downwards. The current source I is located at a point (x_q,y_q,z_q). The governing equation of the electrical potential $v(x,y,z)$ is

$$\nabla\cdot(\sigma(x,y,z)\nabla v(x,y,z)) = -I\delta(x-x_q)\delta(y-y_q)\delta(z-z_q), \tag{1}$$

where δ is the Dirac delta function.
Numerical approximations using equation (1) typically give poor results in the vicinity of the source locations because of steep gradients around the source. A better approach is to remove the effect of the singular potential caused by the source. According to a singularity removal procedure proposed by Lowry et al. (1989), the potential in equation (1) is split into the primary potential v_n caused by the current source in a uniform half-space with the conductvity σ_n and the secondary potential v_a caused by the inhomogeneity of the conductivity with the anomalous conductivity $\sigma_a(x,y,z) = \sigma(x,y,z) - \sigma_n$, giving

$$v(x,y,z) = v_n(x,y,z) + v_a(x,y,z). \tag{2}$$

The primary potential v_n satisfies the partial differential equation

$$\nabla\cdot(\sigma_n(x,y,z)\nabla v_n(x,y,z)) = -I\delta(x-x_q)\delta(y-y_q)\delta(z-z_q). \tag{3}$$

In the case of a uniform half-space, the solution of eq. (3) is

$$v_n = \frac{I}{2\pi\sigma_n r}, \tag{4}$$

if the current source is on the ground surface and $r = \sqrt{(x-x_q)^2 + (y-y_q)^2 + z^2}$ is the distance to the source. Here σ_n is defined as the conductivity of the media at the source point (Zhao & Yedlin, 1996).

With the above procedure, the singularity can be removed completely in the vicinity of the source location. If the background is a uniform half-space, the numerical results are very satisfactory in the whole model domain. However, if the background is a horizontally layered earth or a vertical contact, the numerical results can be distorted near model boundaries. Thus, we make a refinement upon the above described method. We assume that the primary potential is caused by the current source in a horizontally layered earth or in two quarter-spaces. The potential of a vertical contact can be treated easily by the method of images. The potential of a horizontally layered earth is given in Li & Spitzer (2001).
Substituting eqs. (2) and (3) into (1), gives the differential equation for the secondary potential

$$\nabla \cdot (\sigma(x,y,z)\nabla v_a(x,y,z)) + \nabla \cdot (\sigma_a(x,y,z)\nabla v_n(x,y,z)) = 0. \tag{5}$$

In order to solve eq. (5), the boundary conditions must be defined. On the boundaries of the body, with different conductivities, the total potential (v) and the normal component of current ($j_n = \sigma\partial v/\partial n$) must be continuous, where n is the outward normal direction of the boundary interface. It can easily be derived that the secondary potential v_a and $\sigma\partial v_a/\partial n + \sigma_a\partial v_n/\partial n$ must also be continuous at such boundaries. Since there is no current flow through the air-earth interface (Γ_s), where Γ denotes the boundary of the whole model domain and $\Gamma_s \in \Gamma$, we have

$$\frac{\partial v_n}{\partial n} = 0, \qquad \frac{\partial v_a}{\partial n} = 0 \qquad \text{on} \quad \Gamma_s. \tag{6}$$

On the other domain boundaries ($\Gamma_\infty \in \Gamma$), the mixed boundary condition (Dey & Morrison, 1979) may be applied:

$$\frac{\partial v_n}{\partial n} + \frac{\cos(r,n)}{r} v_n = 0, \qquad \frac{\partial v_a}{\partial n} + \frac{\cos(r,n)}{r} v_a = 0 \qquad \text{on} \quad \Gamma_\infty, \tag{7}$$

where r denotes the radial distance from the source location to the boundary and n the outward normal direction at the boundary surface.

For arbitrarily shaped 3D structures, the above boundary value problem has to be solved numerically, for example, using the FE or FD method. In the following section, we derive the FE formulation. For the FD formulation we refer to the different approaches by Dey & Morrison (1979), Zhang et al. (1995) and Spitzer (1995). Find a comparison of these FD formulations in Spitzer and Wurmstich (1999).

3 FORMULATIONS OF THE FINITE ELEMENT EQUATIONS

The FE approximation of the governing equation (5) is performed on a model volume Ω that entirely embraces the volume of the 3D inhomogeneities, and extends far enough in all directions for the anomalous potential to fade out to sufficient smallness on the boundary of Ω. Here, the variational method is used to derive the FE equations. However, the Galerkin method gives exactly the same equations. According to the variational principle, the true solution of a differential equation gives a stationary value to some functional. The functional can be formed by using the minimum theorem (Pridmore et al., 1981). The minimum theorem provides the corresponding functional to eqs. (5) $\sim$ (7) as

$$\begin{aligned} F(v_a) &= \int_\Omega \left[\sigma(\nabla v_a)^2) + 2\sigma_a \nabla v_n \cdot \nabla v_a\right] d\Omega \\ &+ \int_{\Gamma_\infty} \left[\sigma \frac{\cos(r,n)}{r} v_a^2 + 2\sigma_a \frac{\cos(r,n)}{r} v_n v_a\right] d\Gamma. \end{aligned} \tag{8}$$

The model volume Ω is subdivided into hexahedral elements, and the integrals of eq. (8) thus decompose into integrals for each element, in which the conductivity is constant. It reads

$$F(v_a) = \sum_{e=1}^{n_e} \int_{\Omega_e} \sigma (\nabla v_a)^2 d\Omega + \sum_{\Gamma_\infty} \int_{\Gamma_e} \sigma \frac{\cos(r,n)}{r} v_a^2 d\Gamma$$

$$+ \quad 2\left[\sum_{e=1}^{n_e}\int_{\Omega_e}\sigma_a\nabla v_n\cdot\nabla v_a d\Omega+\sum_{\Gamma_\infty}\int_{\Gamma_e}\sigma_a\frac{\cos(r,n)}{r}v_n v_a d\Gamma\right], \tag{9}$$

where Ω_e denotes the volume of a particular element e and Γ_e the surface element on Γ_∞. n_e is the number of hexahedral elements.
We assume that in each hexahedral element the primary and secondary potentials are linear functions of the Cartesian coordinates x, y and z. Then they can be approximated by

$$v_n=\sum_{i=1}^{8}N_i v_{n,i}, \qquad v_a=\sum_{i=1}^{8}N_i v_{a,i}, \tag{10}$$

where $v_{n,i}$ and $v_{a,i}$ are the primary potential and the secondary potential at the corner point i, $i=1,\cdots,8$, in the global coordinates. N_i are the linear shape functions defined by Li (2000) and read

$$N_i=\frac{1}{8}(1+\xi_i\xi)(1+\eta_i\eta)(1+\zeta_i\zeta) \qquad (i=1,\cdots,8), \tag{11}$$

where ξ_i, η_i und ζ_i are the coordinates of the corner point i, $i=1,\cdots,8$, in the local coordinates.
It is possible to transform the global coordinates (x,y,z) to corresponding local coordinates (ξ,η,ζ) by

$$\xi=\frac{2}{a}(x-x_c), \qquad \eta=\frac{2}{b}(y-y_c), \qquad \zeta=\frac{2}{c}(z-z_c), \tag{12}$$

where x_c, y_c and z_c are the coordinates of the center of the hexahedral element, a, b and c are the length, width and height of the hexahedral element. This transformation is a major step in the finite element method which simplifies the evaluation of the integrals of eq. (9). Now the volume integrals in (9) can be analytically evaluated in the local coordinates using eqs. (10) $\sim$ (12).

Similarly, the surface integrals in (9) can be evaluated analytically. Note that here v_n and v_a are determined by linear interpolation of the potentials at four nodes of a rectangular element.

Summing up the integrals over all the elements and assembling the element matrix to a system matrix, results in the following approximation for the functional $F(v_a)$:

$$F(v_a)={v_a}^T\mathbf{K}v_a+2{v_a}^T p \tag{13}$$

where $\mathbf{K}$ is the total system matrix, v_a is the vector of the unknown values of the secondary potentials in all nodal points, and p is the known vector obtained by the last two terms of the right-hand side of eq. (9).
The first variation of the functional with respect to v_a is

$$\delta F(v_a)=2\delta{v_a}^T\mathbf{K}v_a+2\delta{v_a}^T p. \tag{14}$$

The functional is minimized by setting the first variation of the functional to zero, this finally results in the finite element equation

$$\mathbf{K}v_a=-p, \tag{15}$$

where the system matrix $\mathbf{K}$ is symmetric and sparsely occupied by non-zero elements. This system of linear equations is solved numerically using a conjugate gradient method (Hestenes & Stiefel, 1952), which provides the anomalous potential at all nodal points. The total potential is then obtained by adding the anomalous potential to the normal potential.

4 COMPARISONS OF THE FE AND FD SCHEMES

The FE and FD techniques tackle a boundary value problem using very different principles. Whereas the FD formulation directly transfers infinitesimal analytical expressions of the underlying partial differential equations into finite terms, the FE method is based on the variational principle or the method of the weighted residuals. Generally, research focuses on either FE or FD. However, to our knowledge, it is still rather unclear where the particular advantages of each method are if it comes to numerical implementation. Therefore, in this section, we compare the here presented FE approach and an adequate FD scheme by Spitzer et al. (1999) in terms of accuracy and memory requirements. The FD scheme was originally outlined in Spitzer (1995) and uses a formulation that goes back to Brewitt-Taylor & Weaver (1976), but is comparable to Dey & Morrison's approach (1979) (see Spitzer & Wurmstich, 1999).

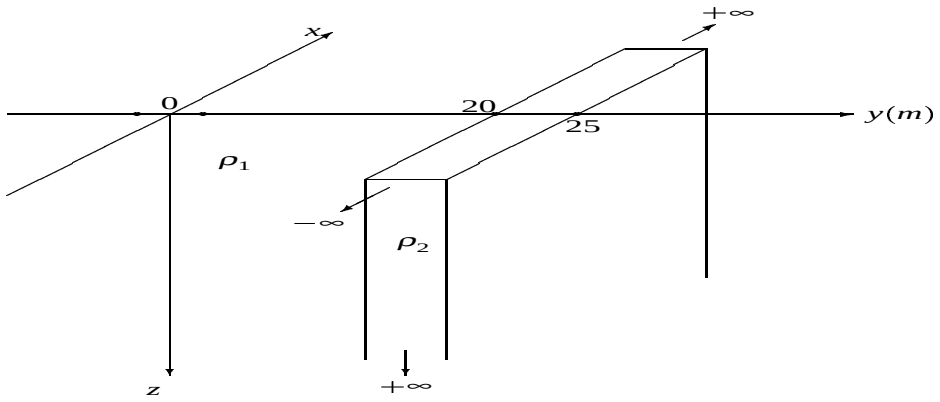

Fig. 1 A vertical dike model.

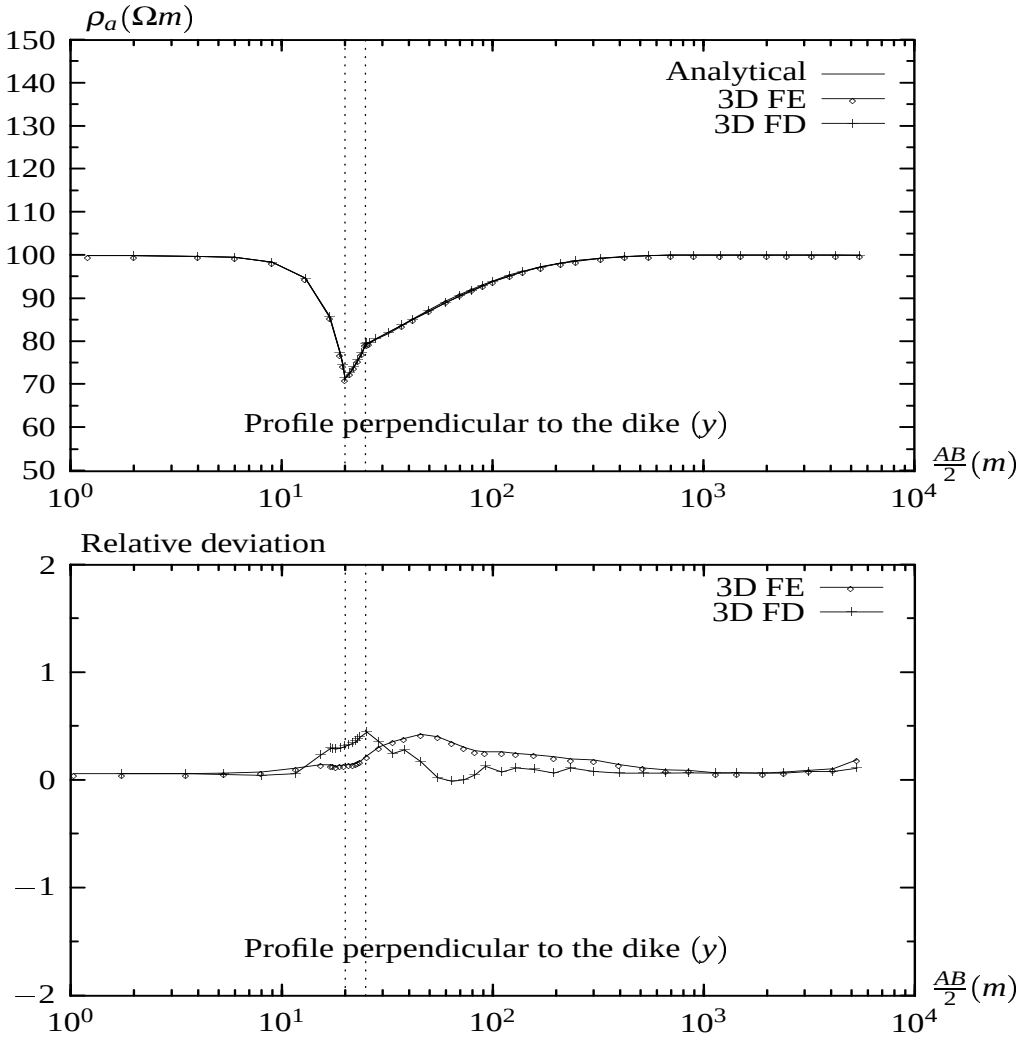

Fig. 2 Apparent resistivity (top) and deviation curve (bottom) of a Schlumberger sounding perpendicular to the dike in fig. 1 (along y-axis).

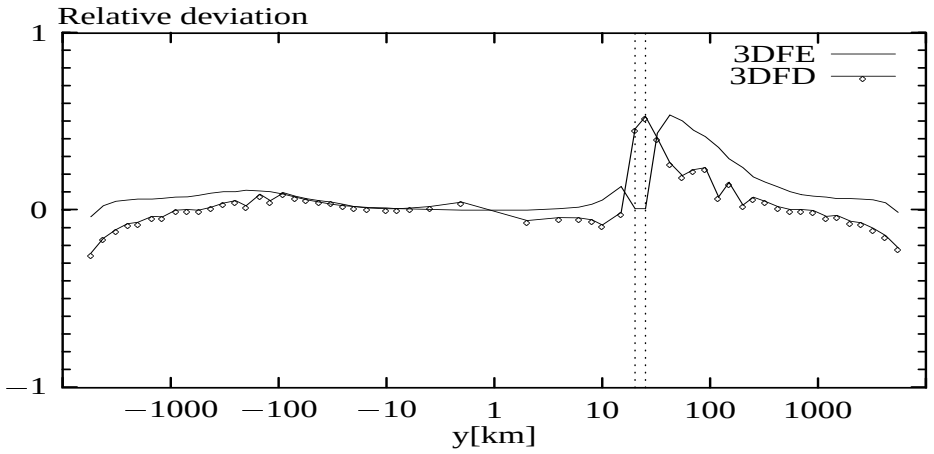

(a)

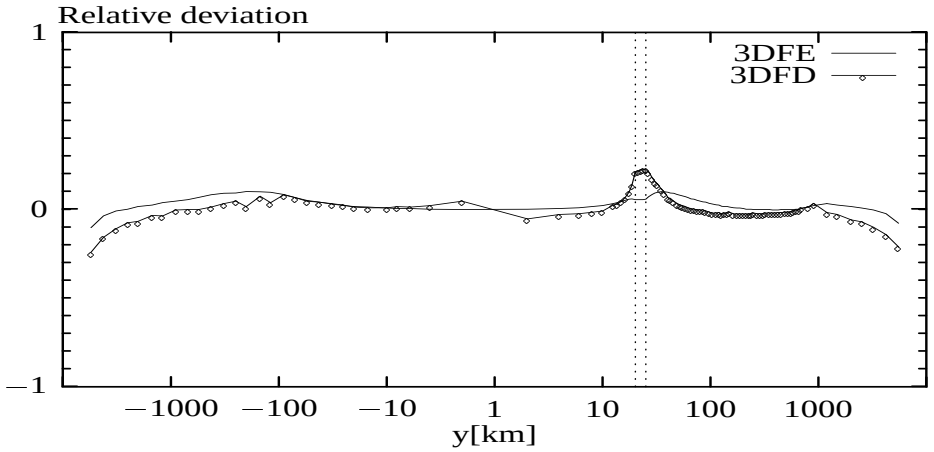

(b)

Fig. 3 Discretization errors of the FE and FD scheme using a coarse grid (a) and a fine grid (b) for the model of the figure 1.

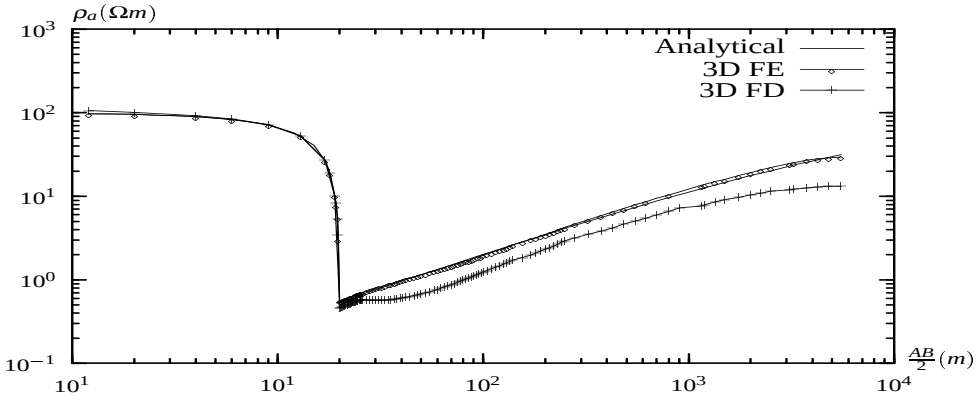

Fig. 4 Appaent resistivity of a pole-pole configuration for a large conductivity contrast of 10^4 for the dike model in fig. 1. After refining the grid, the FE solution becomes accurate again, whereas the FD solution remains unstable.

4.1 Accuracy

The accuracy of the FE and FD scheme is compared for the dike model (Fig. 1). Schlumberger soundings are carried out over the structure. The two current sources are located at $(0m, \pm 1m, 0m)$. The apparent resistivity is calculated exploiting the principle of reciprocity, i.e., current and potential electrodes are interchanged. Thus, the whole Schlumberger sounding curve is obtained by performing only one forward modeling.
The same grid with $73 \times 89 \times 35$ nodes is used for the FE and FD modeling. The modeling domain boundaries are located at $\pm 5500m$ in *x*- and *y*-direction and $5500m$ in *z*-direction. The model is more finely discretized near to the conductivity contrast. Fig. 2 shows the computed FE and FD results of a Schlumberger configuration for a profile perpendicular to the dike (along the *y*-axis). The analytical solution computed by an analytical dike-program (Hanstein, pers. communications) is also shown for comparison. In general, both algorithms provide very accurate results at all nodes. However, the signature of the error distribution is different for each method. Maximum errors between 0.20 and 0.40 per cent occur at $AB/2 = 19 \sim 42m$ for the finite difference solution, whereas for the FE solution the maximum error is between $AB/2 = 32 \sim 120m$. We will discuss these further below.

4.2 Discussion of discretization errors

To investigate the causes of the discretization errors to occur at different places for the FE and FD solution, we perform further numerical tests using the dike model again. An irregular grid with $59 \times 59 \times 30$ nodes is first used and the boundaries are at a distance of $5500m$ in each direction. The potential of a pole-pole configuration is calculated numerically using the FE and FD scheme, respectively. A single current source is located at the origin of the coordinate system. Fig. 3a shows the relative deviations for a profile perpendicular to the dike. Again the error maxima are spatially separated for the FE and FD solutions. If the model discretization is refined at $y = 15 \sim 425m$, the accuracy of the FE scheme is improved considerably, yielding a relative error less than 0.11 per cent over the whole range (Fig. 3b). However, the maximum of the error for the FD scheme remains, although the amplitude is reduced somewhat. These model tests show that there are two origins of discretization errors, i.e., conductivity contrasts and geometric properties. The FD scheme seems to be rather robust with respect to irregular grid geometries, and the FE scheme with respect to conductivity contrasts. These differences are probably related to the treatment of potential and conductivity in assembling the coefficient matrix. A second-order Taylor series expansion of the potential is used for deriving the FD expressions, but in assembling the FE matrix $\mathbf{K}$ it is assumed that the potentials are linear function of the coordinates in each hexahedral element. Thus, a local refinement of grid is necessay in those regions where the potential fields vary steeply to obtain accurate results with the FE modeling. Moreover, in assembling FE coefficients the electrical conductivity is assumed constant over each hexahedron and is equal to the real conductivity of the medium. However, in FD scheme the conductivity value at a grid point is the arithmetric average of eight volume-weighted cell conductivities that surround the grid point. This approximation accounts for increased discretization errors near the conductivity contrast. Uncontrollable numerical instabilities of the FD solution are therefore observed in the case of a very high conductivity contrast. Figure 4 shows the computed FE and FD results of a pole-pole configuration for the conductivity contrast of $\rho_1/\rho_2 = 10000$. The FE solution agrees well with the analytical one after refining the grid adequately. However, it is not possible to restabilize the FD solution.

4.3 Storage size of coefficient matrix

As mentioned in section 3, the coefficient matrix of the FE equations is symmetric and sparse. With the hexahedral element discretization each node has maximal 26 neighbour nodal points. This means that the coefficient matrix generally has 27 non-zero components in each row. Hence 14 non-zero elements need to be stored in each row of the matrix because of the symmetry. For a grid with, e.g., $73 \times 89 \times 35$ nodes, there are about 3.1×10^6 non-zero components to be stored.

Most 3D FD approaches are formulated with a central grid point and its six direct neighbours along the main coordinate axes. This means that the coefficient matrix resulting from FD discretization has maximal 7 non-zero components in each row. Thus, only 4 non-zero components need to be stored in each row because of symmetry. For the above grid of $73 \times 89 \times 35$, there are about 9.1×10^5 non-zero elements to be stored.

In conclusion, the coefficient matrix of FD equations is much more sparse than that of FE equations. The FE scheme requires about 3.4 times as much storage as the FD scheme.

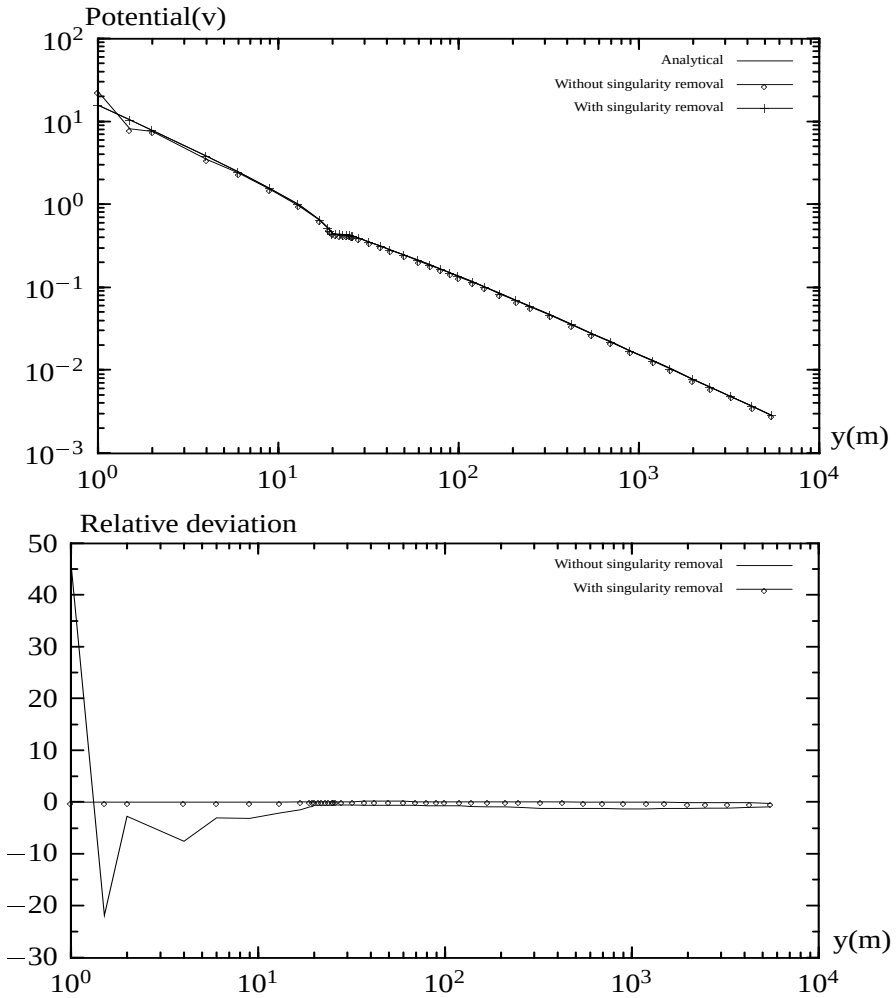

Fig. 5 The effect of singularity removal for a pole-pole configuration perpendicular to the dike depicted in fig. 1 (along *y*-axis).

5 ENHANCED REFERENCE MODELS FOR A MODIFIED SINGULARITY REMOVAL TECHNIQUE

In this section, we first prove the singularity technique to be superior to modeling the total potential. Then we illustrate the advantages of using better suitable reference models for the potential split-up. So far the homogeneous half-space has been used to calculate the normal potential. However, for a wide range of models horizontal layers or vertical contacts are better matching alternatives. We will refer to the former method as the conventional singularity removal technique and the latter as the improved singularity removal technique. We consider three examples: at first the vertical dike model. Here we show the advantage of modeling the secondary potential in general. Then we investigate a cube buried in a two-layered earth and a cube buried near a vertical fault to show the superiority of the improved singularity removal technique. Figure 5 shows the total potential of a pole-pole configuration for a profile perpendicular to the dike (along the *y*-axis). The single current source is located at the origin of the coordinate system. The total potential in the method without singularity removal is obtained by solving the differential equation (1). It is clear from figure 5 that the method without singularity removal produces larger errors than the method with the conventional singularity removal, especially near the current source point. The average error, which is calculated as being the sum of the percent error at all profile nodes divided by the number of nodes, is 2.60 per cent for the FE solution without singularity removal and is 0.10 per cent for the FE solution with singularity removal. This example demonstrates that a secondary potential approach improves the accuracy considerably.

The second model is a cube buried in a two-layered earth shown in the lower left-hand corner of Fig. 6. The first layer has a resistivity of $\rho_1 = 100\Omega m$ and a thickness of $h = 3m$. The second layer is a uniform half-space with a resistivity of $\rho_2 = 10\Omega m$. A conducting cube with a resistivity of $\rho_3 = 10\Omega m$ and

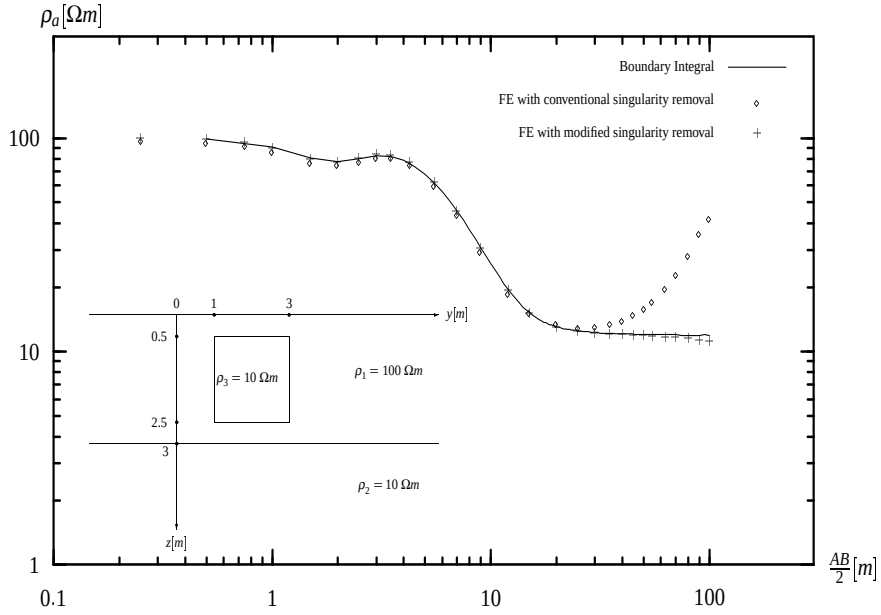

Fig. 6 The effect of singularity removal for a Schlumberger sounding across a cube buried in a two-layered earth.

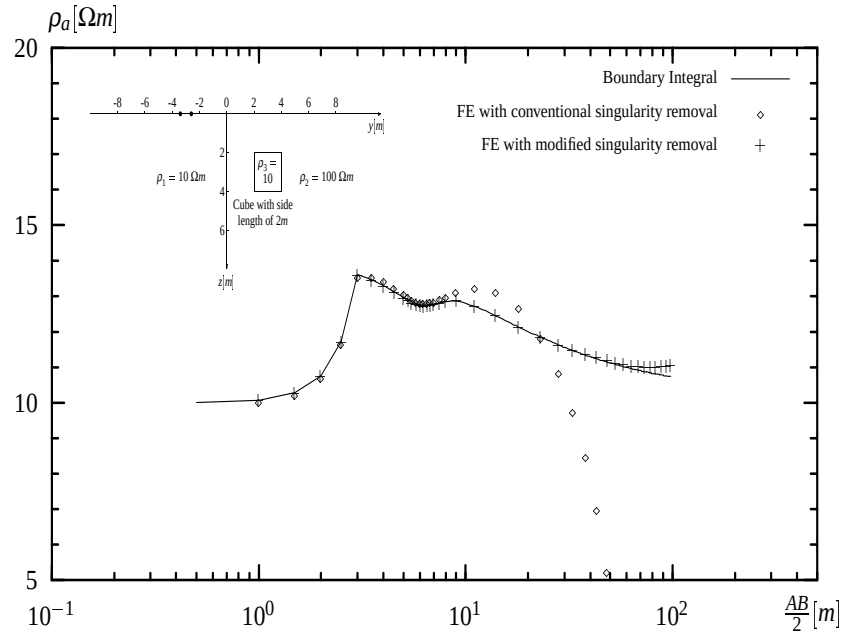

Fig. 7 The effect of singularity removal for a Schlumberger sounding across a cube buried near a vertical contact.

with the side length of $2m$ is embedded in the first layer. The apparent resistivity ρ_a of a Schlumberger sounding is evaluated using the FE method with the modified singularity removal technique, where the two layered earth ($\rho_1 = 100\Omega m$, $h = 3m$ and $\rho_2 = 10\Omega m$) is regarded as the normal structure. In fig. 6 it is compared with the boundary-integral method according to Hvoždara (1995). Both the solutions show good agreement. The numerical result obtained using the FE method with a homogeneous reference background is also shown in figure 6. ρ_a is distorted seriously at large electrode spacings ($AB/2 > 15m$). This example demonstrates that the use of the conventional singularity removal technique using a homogeneous reference model is not appropriate when the background is a layered earth.

The third model is a cube buried near a vertical fault shown in the top left-hand corner of Fig. 7. The apparent resistivity of a Schlumberger sounding is evaluated using the FE method with the modified singularity removal technique. Now the vertical contact is regarded as the normal structure, whose analytical solution is the primary potential. In fig. 7 it is compared again with the boundary-integral method according to Hvoždara & Kaikkonen (1994). The maximum difference of 3.1 per cent occurs at the boundary. The current sources are located at $(0m, -3.4m, 0m)$ and $(0m, -2.6m, 0m)$. The numerical results obtained with the conventional singularity removal technique (i.e. the analytical solution of a uniform half-space with the resistivity of $\rho_1 = 10\Omega m$ is regarded as the primary potential) are distorted seriously when approaching the boundaries.

6 CONCLUSIONS

In this paper we have developed a 3D finite element algorithm for DC resistivity modeling. The singularity removal procedure and mixed boundary conditions are incorporated, and the high degree of accuracy is demonstrated. With the conventional singularity removal technique proposed by Lowry et al (1989) and refined by Zhao & Yedlin (1996), the singularity can be removed in the vicinity of the current source, and the numerical results are very satisfactory over the whole model domain when the background structure is a uniform half-space. However, if the background deviates from the homogeneous case, this technique doesn't work well. We have presented a modified singularity removal technique, where the solution of a horizontally layered earth or a vertical contact is regarded as the primary potential. This technique allows to better adjust to a wide range of models and considerably increases the accuracy toward the boundaries. Especially, horizontal layers are a very common geologic feature, so that the improved singularity removal procedure will be very helpful in practice.

The finite difference and finite element methods are very suitable to model a complex 3D earth. The investigation shows that both differential equation techniques give accurate results, when an appropriate grid is used. Yet, both techniques have individual advantages and disadvantages. On the one hand, the FD method produces larger errors near conductivity contrast than the FE method. On the other hand, the FE method is less robust with respect to grid irregularities. The FD method requires less storage than the FE method, however, it is possible to incorporate tetrahedral elements into the FE technique, which is most suitable to model topography and sloping interfaces. Nevertheless, hexahedral elements are necessary to carray out a significant comparison to the FD technique. For practical application, however, our future work will concentrate on tetrahedral element discretization and the discussion of topographic effects.

7 ACKNOWLEDGMENTS

This work is supported by the Deutsche Forschungsgemeinschaft (Ja 590/18-1). A great part of the computing work has been done at the Geophysical Institute of the University of Göttingen. Thanks to Prof. U. Christensen for providing the necessary facilities. We also wish to thank T. Hanstein and M. Hvož*dara* for providing an analytical dike program and a boundary integral code, respectively.

REFERENCES

Anderson, W.L., 1979. Computer program: numerical integration of related Hankel transforms of orders 0 and 1 by adaptive digital filtering, *Geophysics*, **40**, 1287-1305.

Axelsson, O.,1985. A survey of preconditioned iterative methods for linear systems of equations, *BIT*, **25**, 166-178.

Brewitt-Taylor, C.R., & Weaver, J.T., 1976. On the finite difference solution of two-dimensional induction peoblems, *Geophys. J. R. astr. Soc.*, **47**, 375-396.

Dey, A. & Morrison, H.F., 1979. Resistivity modeling for arbitrarily shaped three-dimensional structures, *Geophysics*, **44**, 615-632.

Hestenes, M.R. & Stiefel, E., 1952. Method of conjugate gradients for solving linear systems, *J. Res. Nat. Bur. Standards*, **49**, 409-436.

Hvoždara, M. & Kaikkonen, P., 1994. The boundary integral calculations of the forward problem for DC sounding and MMR methods for a 3-D body near a vertical contact, *Studia geoph. et geod.*, **38**, 375-398.

Hvoždara, M., 1995. The boundary integral calculation of the DC geoelectric field due to a point current source on the surface of 2-layered earth with a 3-D perturbing body buried or outcropping, *Contr. Geophys. Inst. Slov. Acad. Sci.*, **25**, 7-24.

Kershaw, D., 1978. The incomplete Cholesky-conjugate gradient method for the iterative solution of systems of linear equations, *J. Comp. Phys.*, **26**, 43-65.

Li, Y., 2000. *Finite element modeling of electromagnetic fields in two- and three-dimensional anisotropic conductivity structures*, Ph.D. thesis, Univ. Göttingen.

Li, Y. & Spitzer, K., 2001. *Three-dimensional DC resistivity finite element and finite difference forward modeling in comparison*, submitted to *Geophys. J. Int.*

Lowry, T., Allen, M.B. & Shive, P.N., 1989. Singularity removal: a refinement of resistivity modeling techniques, *Geophysics*, **54**, 766-774.

Meijerink, J.A. & van der Vorst, H.A., 1977. An iterative solution method for linear systems of which the coefficient matrix is a symmetric M-matrix, *Math. Comp.*, **31**, 148-162.

Manteuffel, T.A., 1979. Shifted incomplete Cholesky-factorization, in *Sparse Matrix Proceedings 1978*, edited by Duff, I.S. & Stewart, G.W., SIAM, Philadelphia.

Pridmore, D., Hohmann, G.W., Ward, S.H. & Sill, W.R., 1981. An investigation of finite element modeling for electrical and electromagnetic modeling data in three dimensions, *Geophysics*, **46**, 1009-1024.

Sasaki, Y., 1994. 3-D resistivity inversion using the finite element method, *Geophysics*, **59**, 1839-1848.

Schwarz, H.R., 1991. *Methode der finiten Elemente: eine Einführung unter besonderer Berücksichtigung der Rechenpraxis*, Teubner, Stuttgart .

Spitzer, K., 1995. A 3-D finite-difference algorithm for DC resistivity modeling using conjugate gradient methods, *Geophys. J. Int.*, **123**, 903-914.

Spitzer, K. & Wurmstich, B., 1999. Speed and accuracy in 3D resistivity modeling, in: Oristaglio, M.L. & Spies, B.R. (eds.), *Three-dimensional Electromagnetics*, SEG Book Series " Geophysical Developments " , **7**, Society of Exploration Geophysicists, 161 - 176.

Spitzer, K., Chouteau, M. & Boulanger, O., 1999. Grid-independent electrode positioning for 3D DC resistivity and IP forward modeling, Extended Abstracts Book, 2nd International Symposium on Three-Dimensional Electromagnetics, October 27 - 29, Salt Lake City, Utah, USA, 189 - 192.

Zhang, T., Mackie, R.L. & Madden, T.R., 1995. 3D resistivity forward modeling and inversion using conjugate gradients, *Geophysics*, **60**, 1313-1325.

Zhao, S. & Yedlin, M., 1996. Some refinements on the finite-difference method for 3-D dc resistivity modeling, *Geophysics*, **61**, 1301-1307.

Zhou, B. & Greenhalgh, S.A., 2001. Finite element three-dimensional direct current resistivity modeling: accuracy and efficiency considerations, *Geophys. J. Int.*, **145**, 679-688.